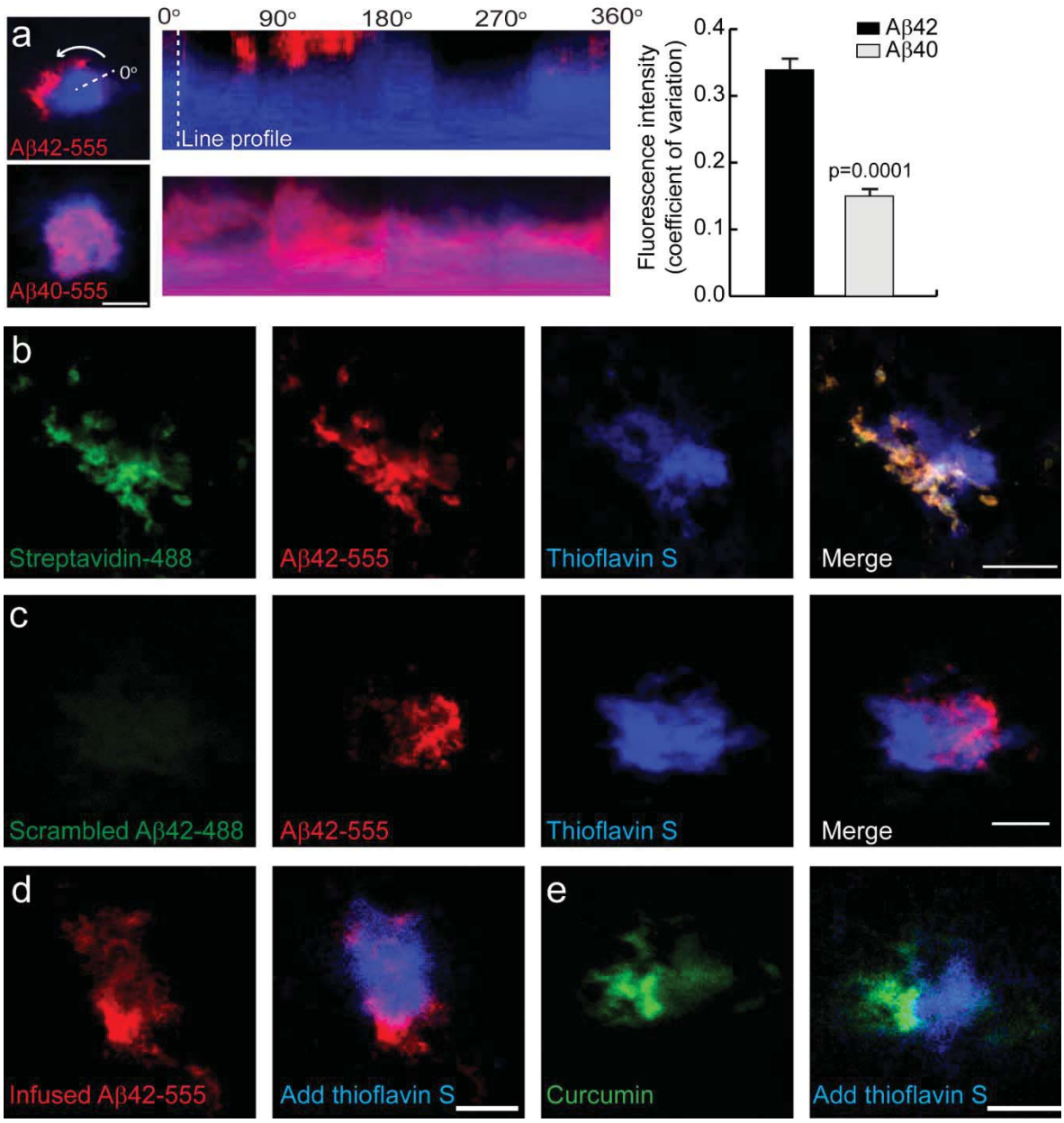

Supplementary Figure 1: Various controls for determining the specificity of the Aβ42 hotspot binding

(a) Comparison of the binding pattern of Aβ42 and Aβ40. Fluorescence line profile of red channel along plaque radii (0° to 360°) was measured from the center of the plaque, as shown in left panels. Coefficient of variation of all line profiles indicates the degree of heterogeneity in the binding as a result of the presence of Aβ42 hotspots compared to the homogenous pattern for Aβ40. N>40 plaques from 6-month-old mice. Data represents mean ± s.e.m. (unpaired t-test, $t=_{(54)}4.104$). **(b)** *In vivo* subarachnoid infusion of biotinylated Aβ42 shows an identical binding pattern to that of Aβ42-555, demonstrating that the hotspot is not an artifact due to the tagged fluorophore. (**c**) Scrambled Aβ42-488 shows no binding to the amyloid plaque indicating the Aβ42 hotspot is not due to non-specific protein interactions. (**d**) Aβ42 infusion in vivo and imaging of the fixed tissue shows a clear hotspot pattern. Subsequent application of Thioflavin S and reimaging of the same plaque did not show any changes in the hotspot. This demonstrates that the hotspot is not the result of competition due to pre-labeling plaques with small moleculedyes. (**e**) Application of Curcumin in fixed slices demonstrates a clear hotspot pattern. Subsequent application of Thioflavin S and reimaging demonstrates that the hotspot pattern is not due to competitive binding between Curcumin and Thioflavin S.

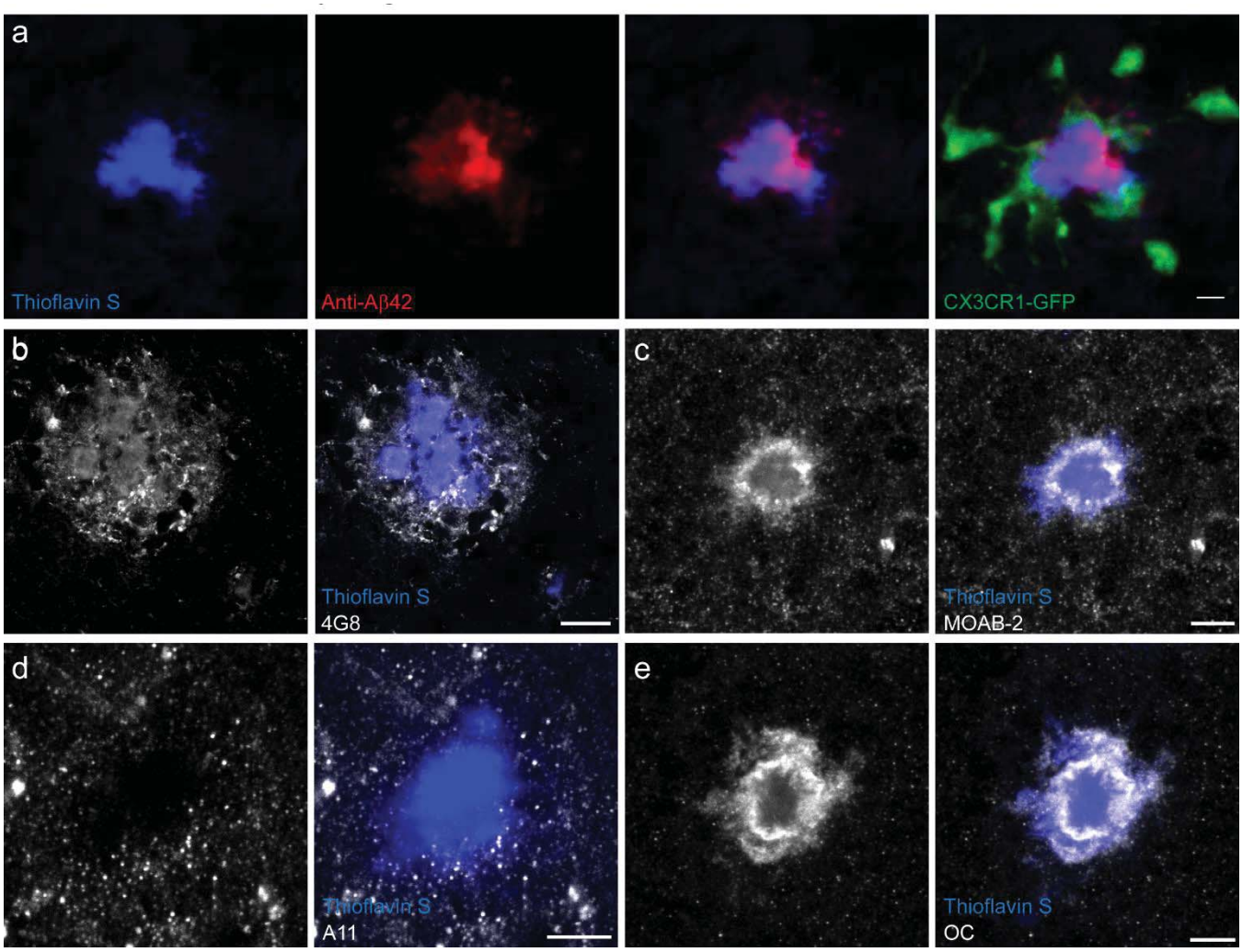

Supplementary Figure 2: Immunohistochemistry of different endogenous Aβ species in brain slice

(**a**) Anti-Aβ42 immunostaining in Cx3CR1-GFP x 5xFAD mice showed endogenous Aβ42 is highly concentrated in plaque microregions lacking microglia process, matching the Aβ42 hotspot seen with exogenous applied Aβ42. (**b** and **c**) Antibodies recognizing Aβ17-24 (4G8, panel **b**) or pan Aβ (MOAB-2, panel **c**) did not highlight the hotspot. (**d** and **e**) Conformation specific amyloid antibodies recognizing pre-fibrillar oligomers (A11, panel **d**) or fibrillar oligomers (OC, panel **e**) did not show hotspot labeling pattern. Scale bars: 5µm in all panels. Based on our results, it is reasonable to suggest that Aβ has adopted a protofibrillar conformation because this region is virtually devoid of any Thioflavin S signal (a robust marker of fibrillar amyloid, figure **4**) and co-localizes with a small molecule dye such as Curcumin, which has been shown to interact with oligomers and proto-fibrils in vitro (Figure **5**). Conformation specific amyloid antibodies (A11 and OC), characterized *in vitro* with synthetic peptides, bind pretty broadly to the plaques and areas between plaques. Thus, they do not show any regional specificity like the "hot spots". As these results exclude the fibrillar and oligomeric amyloid, we conclude that the "hotspots" are of predominant "protofibrillar" conformation.

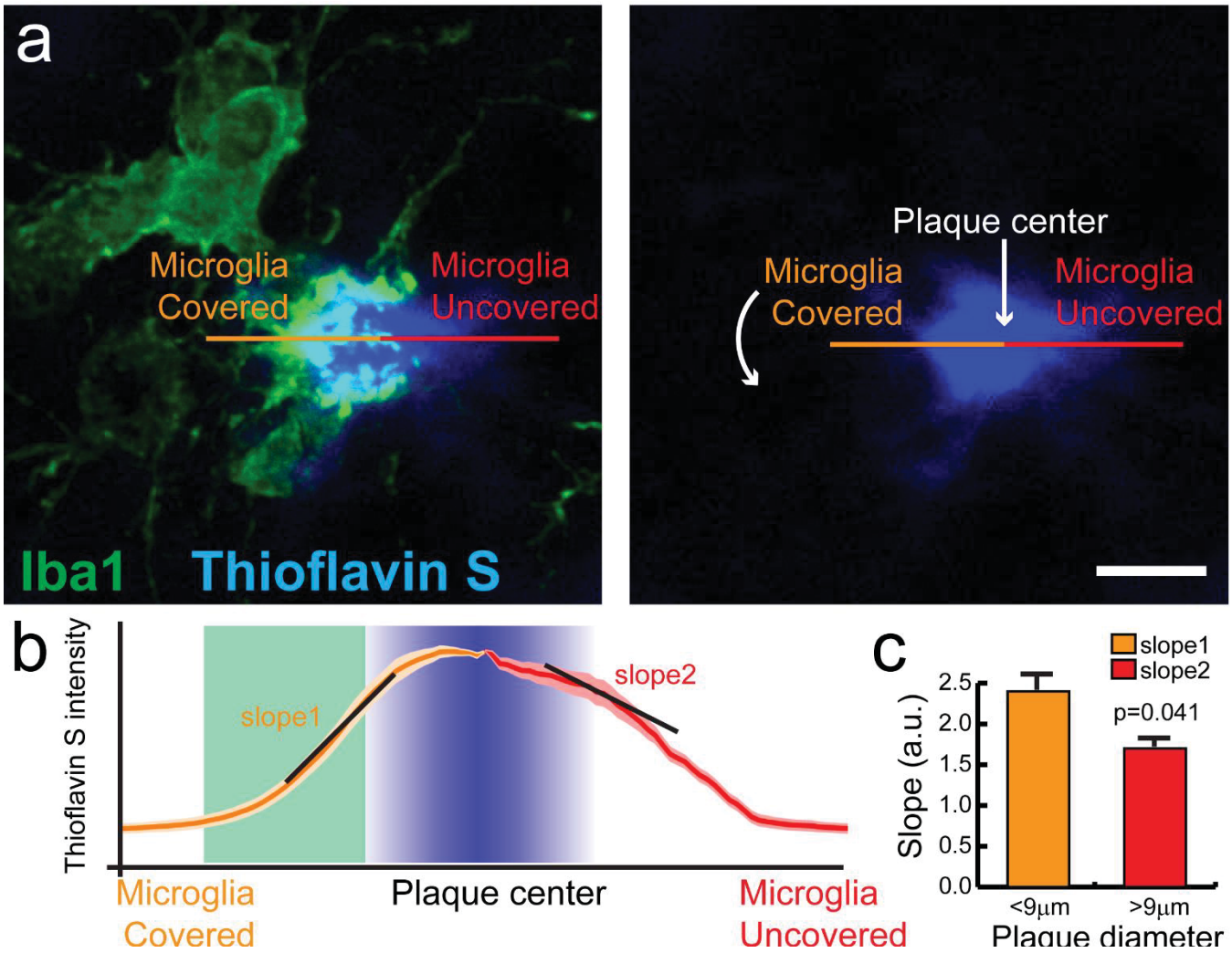

Supplementary Figure 3: Plaque areas covered by microglia processes have greater amyloid compaction

(**a**) The schematic drawing (right panel) shows the method for fluorescence profile analysis. A line selection is made from the centroid of the plaque and fluorescence intensity in the Thioflavin S channel is measured in every pixel along the line. This measurement is obtained for line selections at every angular degree and categorized into the microglia covered or uncovered groups. (**b**) Fluorescence distribution highlighting the slopes of the TS fluorescence intensities next to microglia covered (green shaded rectangle) and microglia uncovered areas. Data represents mean±s.e.m. (**c**) Quantification of Thioflavin S fluorescence slope (Fluorescence change rate) in areas with and without microglia coverage. The slope corresponds to the best-fitted line of 20 data points centered at the plaque thresholded boundary. N=40 plaques from two 6-month-old 5xFAD mice. Data was collected from plaques 10 microns or smaller. Data represents mean±s.e.m. (unpaired t-test, t=2.892).

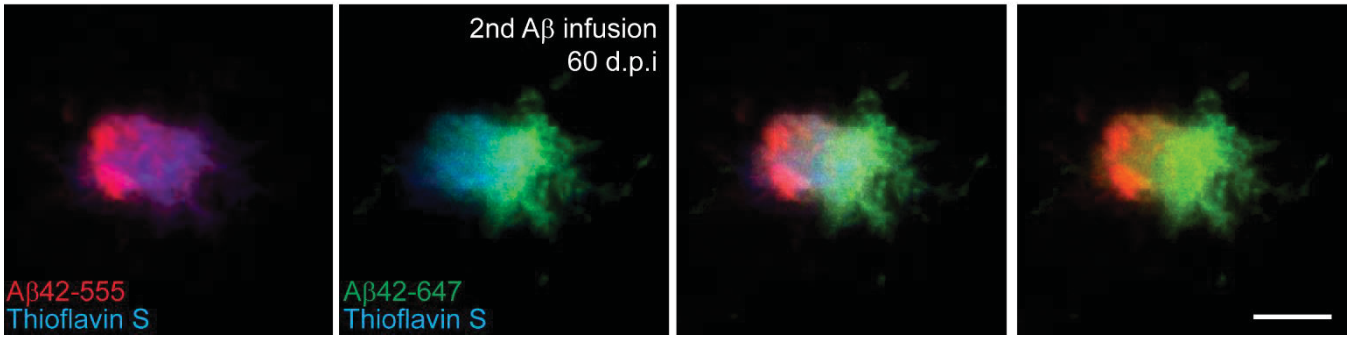

Supplementary Figure 4: Example of Aβ42 hotspot relocation during a 60 day interval

Aβ42-555 was injected through subarachnoid space to label the hotspot at the initial time-point. 60 days later the brain tissue was harvested 1d after the second subarachnoid injection of Aβ42-647. Confocal images showthe appearance of two separate hotspots on a Thioflavin S-labeled amyloid plaque in this example. Scale bar: 5µm.

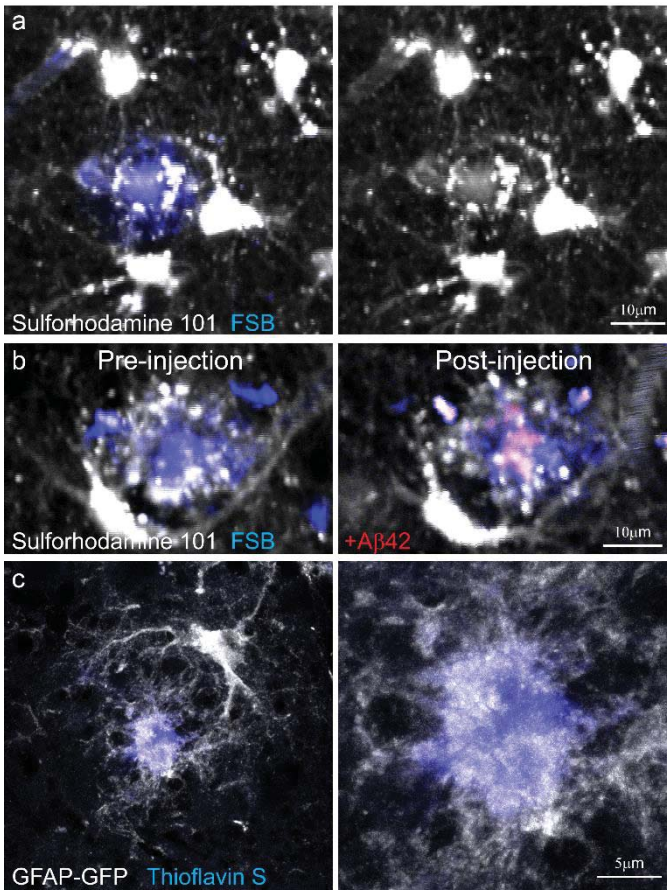

Supplementary Figure 5: Astrocyte processes do not affect Aβ42 hotspot locations despite robustly wrapping around amyloid plaques

(**a**) *In vivo* two-photon imaging of astrocyte processes around amyloid plaques. Astrocytes were labeled following an I.V. injection of sulforhodamine 101. (**b**) Time-lapse images of Aβ42 binding to amyloid plaque. Despite the extensive amount of astrocytic processes covering the plaque perimeter, they do not show any spatial correlation to Aβ42 hotspot. (**c**) High resolution confocal images of fixed brain slices. Astrocytes were labeled by crossing 5xFAD mice with GFAP-GFP mice. In contrast to the GFAP immuno-label, the cytoplasmic GFP-labeling of fine astrocytic processes reveal a near complete coverage of the plaque perimeter.

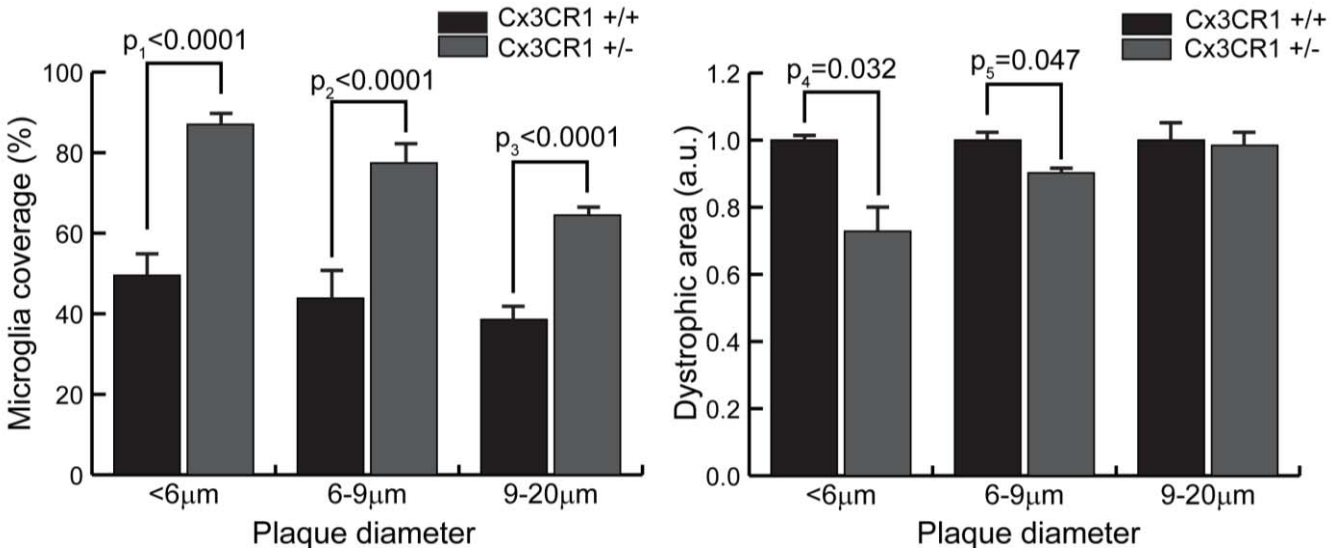

Supplementary Figure 6: CX3CR1 knock-down in 5xFAD mice increases microglia coverage and reduces neuritic dystrophy.

Quantification of microglia coverage and dystrophic area as a function of CX3CR1 genotype and plaque size. $t1=_{(155)}8.872$, $t2=_{(131)}12.63$, $t3=_{(120)}9.190$, $t4=_{(255)}2.159$, $t5=_{(256)}1.992$. N>60 plaques in each size group from each of the 3 mice for each genotype.

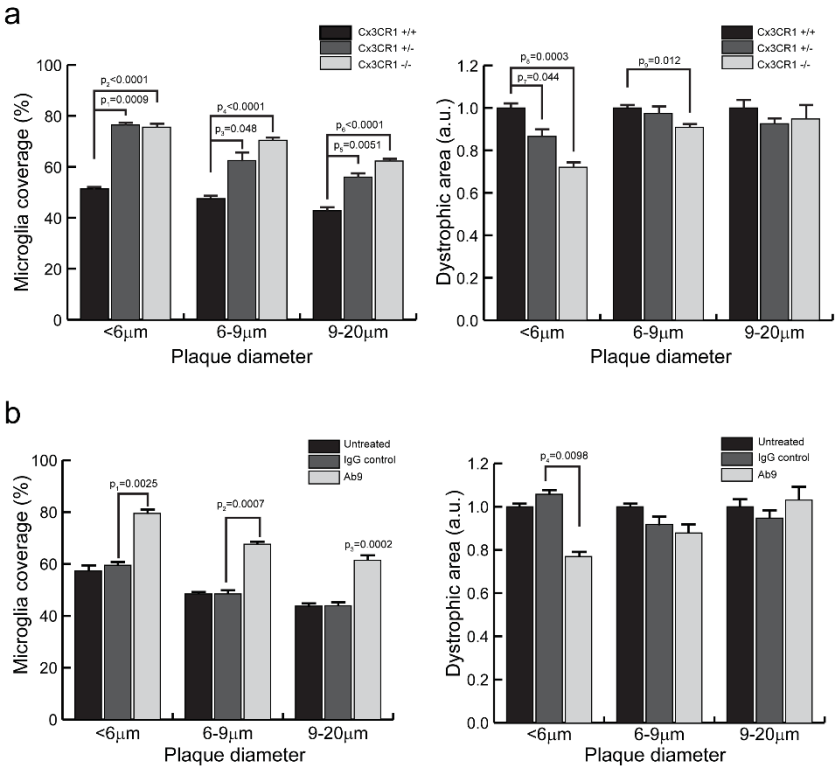

Supplementary Figure 7: Statistical analysis of microglia coverage and neuritic dystrophy utilizing animals instead of individual plaques as observation variables

(**a**) Quantification corresponding to Fig. 8 **b** and **c**. t1=$_{(6)}$6.126, t2=$_{(8)}$7.538, t3=$_{(6)}$4.954, t4=$_{(8)}$11.25, t5=$_{(6)}$4.293, t6=$_{(8)}$10.46, t7=$_{(6)}$4.062, t8=$_{(8)}$6.084 and t9=$_{(8)}$3.221. N=5, 3 and 5 for Cx3CR1 +/+, Cx3CR1+/- and Cx3CR1 -/-, respectively. (**b**) Quantification corresponding to Fig. 8 **e** and **f**. t1=$_{(10)}$4.016, t2=$_{(10)}$4.811, t3=$_{(10)}$5.862 and t4=$_{(10)}$3.181. N=5, 5 and 7 for untreated, IgG control and Ab9 group, respectively.

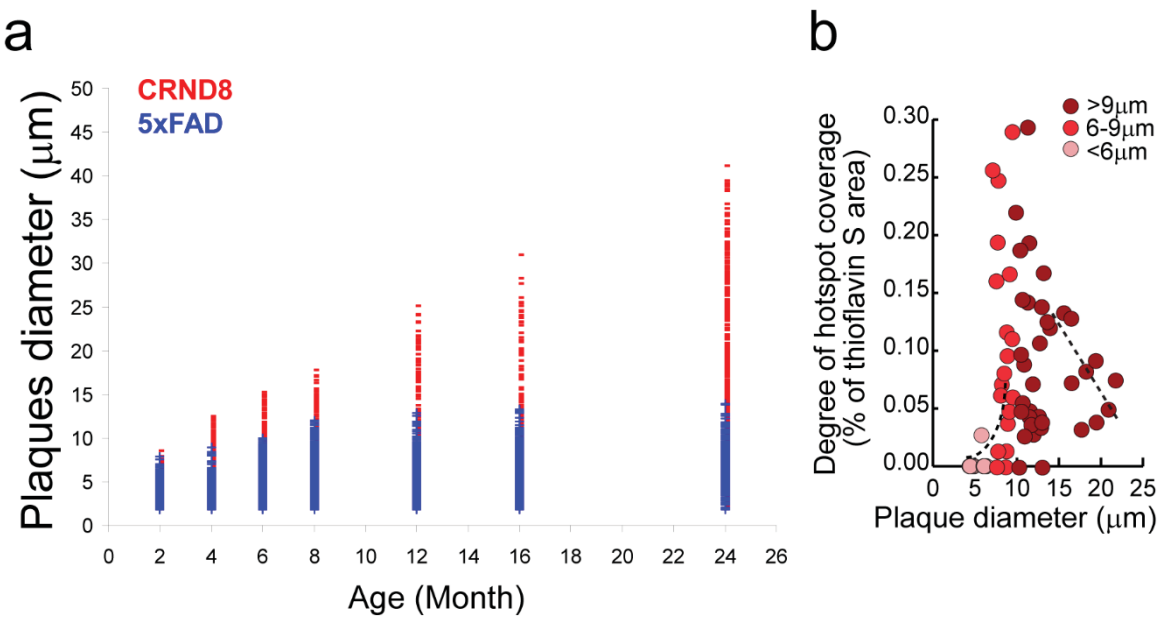

Supplementary Figure 8: Amyloid plaque size distribution in 5xFAD and CRND8 transgenic mice at different ages

(a) Distribution of fibrillar amyloid plaque size in 2 to 24 month old 5xFAD (blue) and CRND8 (red) mice. In 3-4 animals per age group, cortical and hippocampal plaques in fixed brain slices were labeled by Thioflavin S and visualized by confocal microscopy. These data indicate that plaque sizes plateau in the 5xFAD mice as early as 8 months of age. In contrast, plaque size in the CRND8 mice progressively become larger throughout the lifetime of the animal. (b)Plaques from 8 month old 5xFAD mice (n=3). Mice received subarachnoid infusion of fluorescently-labeled Aβ42. Hotspots were imaged in fixed brain slices with confocal microscopy. The theresholded Aβ42 binding area was plotted against the thresholded Thioflavin S area.

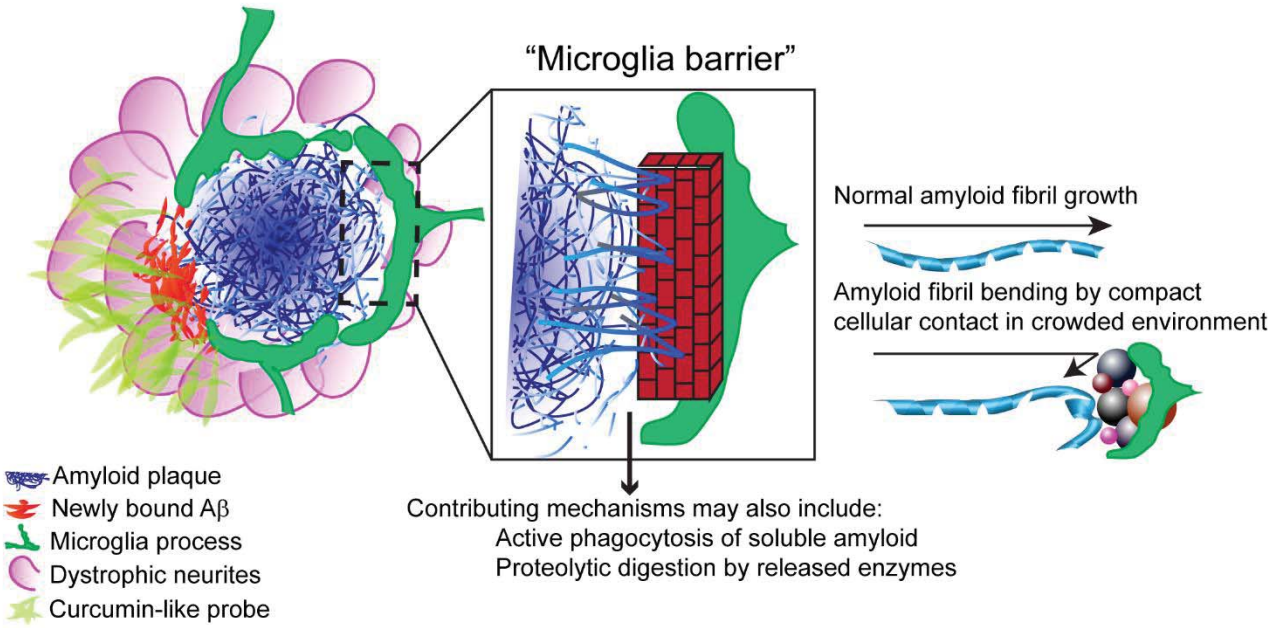

Supplementary Figure 9: Proposed mechanisms of the microglia barrier

Schematic diagram depicts areas covered and not covered by microglia. While the precise cellular mechanism is difficult to dissect, our data supports the following: 1) microglia act as a physical barrier that prevents the outward expansion of fibrillar plaques as strongly suggested in Figure **4** and Supplementary Figure **4**. 2) This leads to microregions with higher amyloid fibril packing density (higher Thioflavin S fluorescence). Such areas have lower affinity for infused or endogenous Aβ42 as demonstrated in our experiments (Figs. **2** and **3**). 3) Areas not covered by microglia have greater Aβ42 binding because the density of amyloid fibrils is lower (Fig. **4**). The precise reason for the grater affinity to these uncovered areas is not clear. However, these regions have low fibrillar content (low Thioflavin S) and it has been shown in vitro that when low amounts of fibrils are present in solution they efficiently catalyze the polymerization of oligomers and protofibrils from soluble monomers (PMID 23703910), and over time these small polymers convert into amyloid fibrils (PMID 21804535). Given the propensity of Aβ42 to aggregate compared to Aβ40, it is likely that the formation of nascent fibrils or extension of growing fibrils is primarily driven by Aβ42. Dyes such as curcumin have a very high affinity for these particular regions and thus can be used to highlight them. 5) Neuronal processes near areas not covered by microglia processes are exposed to higher concentrations of protofibrillar Aβ42 which leads to greater neuritic injury. On the other hand, areas that are thoroughly covered by microglia processes create a crowded microenvironment that is unfavorable for Aβ polymerization.

Discussion

Lines of evidence in favor of a microglia protective role rather than a simple physical displacement explaining the asymmetry in the location of the neuritic dystrophy observed in our study:

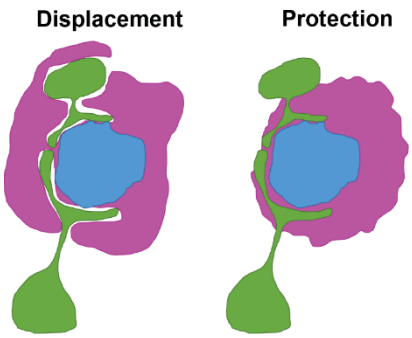

1) Our in vivo imaging data clearly shows that there is a reduced rate of dystrophic neurite formation in the microglia covered regions (**Fig. 7g-h**). This result is inconsistent with the possibility of simple physical displacement and strongly suggests that the microglia barrier is neuroprotective.
2) If mere displacement was the explanation then we would expect the dystrophic neurites to be displaced in all directions and eventually homogeneously surround the plaque, even behind microglia processes or cell bodies, with the exception of areas with microglia processes which would exclude neuronal processes (see adjacent diagram). Instead of that, we see the polarization of dystrophy away from microglia processes (**Fig. 7**) and do not see dystrophy surrounding the processes.
3) The displacement model predicts that the total amount of plaque-associated neuritic dystrophy should not change when manipulating the microglia barrier, but merely its location. However our data with CX3CR1 knockout mice or anti-Aβ passive immunization leads to increased microglia coverage around individual plaques and correlates with an overall reduction in plaque-associated neuritic dystrophy. Furthermore, in our aging experiments, we see the opposite, in which a reduction in microglia correlates with an overall increase in dystrophy area, rather than simply changes in its polarization or location as would occur if mere displacement was the explanation.
4) It is also important to note that plaque regions not covered by microglia are not devoid of other cellular structures just because they are not labeled or visualized. There are astrocyte processes and cell bodies (see **Supplementary Fig. 5**) as well as oligodendrocytes, NG2 cells, and capillaries, all tightly packed and with the capacity to physically displace neuronal processes. This would lead to a multidirectional displacement rather than the polarized one we observe.